



## **Deriving cool flame propagation speeds by means of an ozone-seeded, stagnation plate burner configuration**

Thomas Panaget, Pierre Bragança, Bertrand Lecordier, Amaury Lahccen, Christophe Cuvier, Sébastien Batut, Yann Fenard, Guillaume Vanhove, Laure Pillier

### **► To cite this version:**

Thomas Panaget, Pierre Bragança, Bertrand Lecordier, Amaury Lahccen, Christophe Cuvier, et al.. Deriving cool flame propagation speeds by means of an ozone-seeded, stagnation plate burner configuration. *Fuel*, 2024, 362, pp.130766. <10.1016/j.fuel.2023.130766>. <hal-04376944>

**HAL Id: hal-04376944**

**<https://hal.science/hal-04376944v1>**

Submitted on 9 Jan 2024

**HAL** is a multi-disciplinary open access archive for the deposit and dissemination of scientific research documents, whether they are published or not. The documents may come from teaching and research institutions in France or abroad, or from public or private research centers.

L'archive ouverte pluridisciplinaire **HAL**, est destinée au dépôt et à la diffusion de documents scientifiques de niveau recherche, publiés ou non, émanant des établissements d'enseignement et de recherche français ou étrangers, des laboratoires publics ou privés.



Distributed under a Creative Commons CC BY 4.0 - Attribution - International License

# Deriving Cool Flame Propagation Speeds by Means of an Ozone-Seeded, Stagnation Plate Burner Configuration

Thomas Panaget<sup>a,b,e</sup>, Pierre Bragança<sup>c</sup>, Bertrand Lecordier<sup>d</sup>, Amaury Lahccen<sup>e</sup>,  
Christophe Cuvier<sup>c</sup>, Sébastien Batut<sup>e</sup>, Yann Fenard<sup>e</sup>, Guillaume Vanhove<sup>e</sup> and  
Laure Pillier<sup>e,\*</sup>

<sup>a</sup> Univ. Lille, Inserm, CHU Lille, Institut Pasteur Lille, U1167 – RID-AGE – Facteurs de risque et déterminants moléculaires des maladies liées au vieillissement, F-59000 Lille, France

<sup>b</sup> Junia, Health and Environment, Laboratory of Sustainable Chemistry and Health, F-59000 Lille, France

<sup>c</sup> Univ. Lille, CNRS, ONERA, Arts et Métiers Institute of Technology, Centrale Lille, UMR 9014 - LMFL - Laboratoire de Mécanique des Fluides de Lille - Kampé de Fériet, F-59000 Lille, France

<sup>d</sup> Normandie Univ., UNIROUEN, INSA Rouen, CNRS, CORIA, 76000 Rouen, France

<sup>e</sup> Univ. Lille, CNRS, UMR 8522 - PC2A - Physicochimie des Processus de Combustion et de l'Atmosphère, F-59000 Lille, France

## Full length article

### Abstract

This study aims to investigate the feasibility of experimental determination of DME/O<sub>2</sub>/O<sub>3</sub> cool flame propagation speeds using Particle Image Velocimetry (PIV) in a stagnation plate burner operated at atmospheric pressure. A specific PIV data analysis procedure was developed in order to improve the accuracy of the measurements in this particular configuration. Five flame conditions, with equivalence ratio varying from 0.3 to 0.5 and ozone mole fraction varying from 1.5 to 2% were investigated to compare experimental results with kinetic modeling. Three ozone-submechanisms, respectively from Jian et al. (Jian et al., 2022), Halter et al. (Halter et al., 2011) and Zhao et al. (Zhao et al., 2016), were coupled with our previously developed DME mechanism (Panaget et al., 2021) and used to compare experimental and simulated axial velocity profiles. Results show that a thoughtful choice of the ozone-submechanism is of particular importance in predicting an accurate cool flame velocity in these conditions. A numerically assisted non-linear extrapolation method is proposed for the determination of the unstrained cool flame speed  $S_{u,0}$ . Additionally, simulations for which the plate temperature reaches the maximal flame temperature (adiabatic conditions) were performed, demonstrating a negligible effect of the plate temperature on the determined  $S_{u,0}$ . A kinetic analysis is also presented to highlight the most sensitive chemical reactions influencing the reference cool flame speed  $S_{u,ref}$ , showing the preponderant role of the fuel low temperature chemistry.

**Keywords:** Cool flame, Propagation speed, Low temperature combustion, Particle Image Velocimetry, Ozone assisted combustion

\*Corresponding author: laure.pillier@univ-lille.fr

## 1. INTRODUCTION

From their discovery two centuries ago [1] to their recent observation under micro-gravity conditions [2], cool flames raised a number of issues throughout the years [3,4]. They are known to play a critical role in advanced combustion technologies [5] as they control both autoignition and assisted-ignition processes in the low-temperature combustion regime. Flame propagation speeds are fundamental parameters in combustion due to their influence on the rate of heat release within the reaction zone of flames. Cool flame speeds were numerically investigated by Ju et al. [6,7] and by Zhao et al. [8]. Using dimethyl ether (DME)/O<sub>2</sub> mixtures in both freely-propagating and counter-flow conditions, it was reported that cool flame speeds typically range from 6 to 20 cm.s<sup>-1</sup>, depending on the experimental conditions. Interestingly, they are almost insensitive to the equivalence ratio within their stability range, while their hot flames counterparts are known to be highly dependent on this parameter. Numerical investigations of the effect of ozone on the cool flame speed have shown that it increases as the ozone concentration increases, as in the case of hot flames [9,10].

To the best of our knowledge, experimental cool flame propagation speeds were only reported under microgravity conditions [11] or at sub-atmospheric pressure by the Belmont group [12–16]. Foster and Pearlman [11] measured the speed of a propane/O<sub>2</sub> cool flame at low-pressure and microgravity conditions, using the spherically-propagating flame method. It was however observed that heat was released by pre-ignition of the mixture, prior to the cool flame formation. Thus, the measurement could not be used to determine the propagation speed of the propane cool flame. Recent work from Belmont group at the University of Wyoming [12–16] showed the feasibility of measuring cool flame speeds using a Hencken Burner operated at sub-atmospheric pressure. They reported low pressure data for ozone-seeded cool flames of dimethyl ether, propane and *n*-heptane. This method consists of varying the gas inlet flow rate while keeping the equivalence ratio fixed, and measuring the position of the flame

above the burner by excited formaldehyde chemiluminescence or formaldehyde planar laser induced fluorescence (PLIF). Two distinct regimes are then identified: a/ a first regime where the flame remains anchored to the burner by the heat losses, and where the variation of the inlet flow rate causes only a minimal variation of the flame position; b/ a second regime, where the flame detaches from the burner surface and is considered freely-propagating and nearly adiabatic, the heat transfer being considered negligible. In this case, the flame position varies linearly with the inlet flow rate. The transition between these two regimes was suggested to provide a reasonable estimate of the cool flame speed. This method was validated for hot flames by comparing flame speeds measured by Particle Image Velocimetry (PIV) [16,17] and data from the literature and simulations. The cool flame speeds obtained experimentally by Hajilou et al. were simulated with different kinetic models [13-15] using freely-propagating flame simulations.

Ozone has been widely used in experimental cool flames studies [15,18] as its thermal decomposition releases highly reactive oxygen atoms at temperatures close to 450 K at the atmospheric pressure, facilitating the initiation of low-temperature reactivity [19]. Several ozone specific submechanisms have been developed in the past years, and are commonly coupled with hydrocarbon mechanisms to describe the decomposition of ozone and its impact on combustion [20–22]. Knowing the important influence of ozone on the combustion process, it is important to wisely choose the ozone submechanism when simulating the behaviour of ozone-seeded cool flames.

In this work, we investigated the feasibility of measuring atmospheric pressure lean DME/O<sub>2</sub>/O<sub>3</sub> cool flames propagation speeds from the measurements of the axial velocity profiles using PIV in a newly implemented stagnation plate burner [23]. A specific PIV data analysis procedure, developed in order to improve the accuracy of the measurements, is presented. Five different flames conditions have been studied with equivalence ratio varying

from 0.3 to 0.5 and O<sub>3</sub> mole fraction from 1.5 to 2%. Comparison with simulations is performed using three different O<sub>3</sub>-submechanisms from the literature [20–22] coupled to a detailed kinetic mechanism recently developed in our group [23] for DME low temperature combustion. The performance of the coupled mechanisms is first assessed in predicting experimental axial velocity profiles in the strained cool flames, then a method to extract the unstrained propagation speed is proposed. Finally, a kinetic analysis is performed to highlight the most sensitive chemical reactions influencing the cool flame speed.

## **2. EXPERIMENTAL AND NUMERICAL METHODS**

### **2.1. Experimental setup for PIV measurements**

The stagnation plate burner used in the present study has already been extensively described in a previous study [23], and will therefore only briefly be presented in the present work (Figure 1). It consists of a stainless-steel body, with a coaxial converging nozzle of an inner diameter of 10 mm for the DME/O<sub>2</sub>/O<sub>3</sub> mixture. This mixture is injected through four orthogonal inlets and flows through a stainless-steel porous disc before entering the convergent section of the burner. This geometry is chosen as it provides a laminar and uniform flow at the burner exit. A N<sub>2</sub> co-flow exits through a 20 mm internal diameter co-axial nozzle also equipped with a stainless-steel porous section to protect the cool flames from external perturbations. The burner body is kept at a constant temperature of 300 K by a temperature-regulated water circulation system, and is operated at atmospheric pressure. A cylindrical heated plate, with a diameter of 65 mm and a thickness of 8 mm, is placed at 13 mm from the burner nozzle, with a strictly parallel geometry, and is heated at  $600 \pm 0.1$  K. Gas flow rates are controlled by Bronkhorst mass flow controllers, whose calibration was performed using DryCal DC-Lite Primary Flow Meters. Part of the O<sub>2</sub> flows through two ozone generators (BMT Messtechnik GMBH) arranged in parallel. The ozone mole fraction is measured at the entrance of the burner

with a Teledyne API 452 ozone analyser, the relative uncertainty on the reported ozone concentrations being  $\pm 0.02\%$  for every studied condition. The ozone mole fraction at the burner outlet has been measured both in reactive and non-reactive conditions using an Omnistar GSD 301 O<sub>2</sub> Pfeiffer Vacuum mass spectrometer, showing no ozone reactivity or decomposition before the burner outlet.

Measurements of the axial velocity profiles between the burner and the plate are performed using the PIV technique which is based on the diffusion of illuminated particles seeded in the flow. In our case, part of the oxygen flows through a liquid atomizer, allowing the seeding of small particles in the flow. Silicon oil, provided by Chem-Lab, is chosen for its well-defined properties (viscosity, surface tension, etc.) and its high vaporization temperature, around 600 K. In the studied conditions, the temperature does not exceed 900 K downstream from the flame, and the temperature in the flame front is around 600 K [23]. The particle diameter is estimated to be in the range 1 – 5  $\mu\text{m}$ , as usually met for this kind of atomizer [24]. The flame position did not change with the addition of particles, demonstrating that the seeding by silicon oil droplets does not affect the cool flame speed. The use of silicon oil is therefore well adapted for such PIV measurements, as will be demonstrated further later in this manuscript.

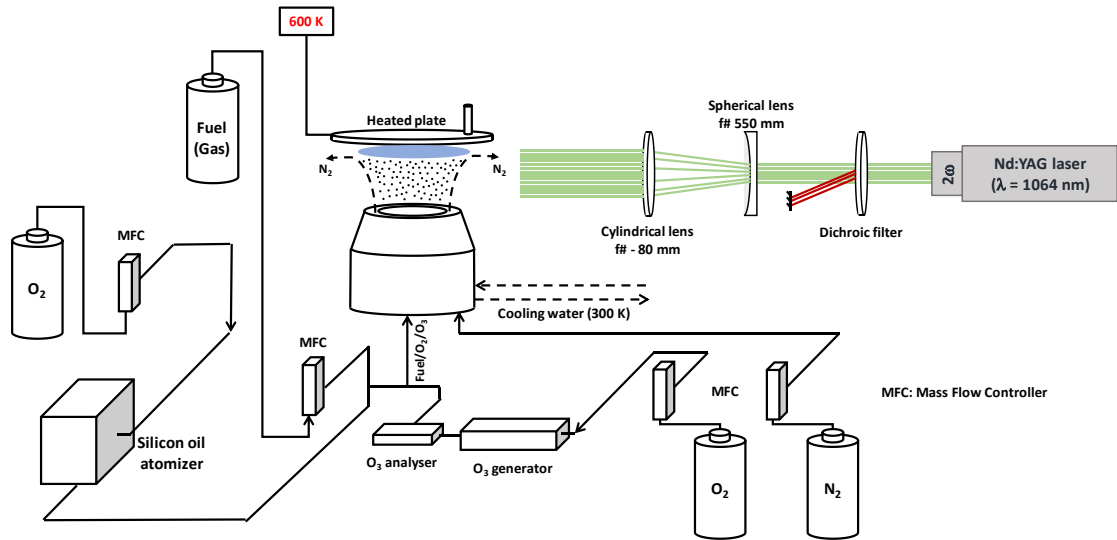


**Figure 1.** Schematic diagram of the experimental setup.

Particles are illuminated by a dual cavity Nd:YAG Splitlight Compact laser from Innolas, delivering a 50 mJ pulse at 532 nm, at a frequency of 10 Hz. The laser sheet, centred on the burner, is generated using spherical (f# 550 mm) and cylindrical (f# - 80 mm) lenses. The laser sheet dimensions are  $\sim 12$  mm height x 600  $\mu$ m thick. The particles displacement between two laser pulses is captured using a LaVision Scmos camera of 2560 by 2160 pixels, equipped with a 105 mm Nikkor lens at an aperture of f#8, the resulting magnification being equal to 20  $\mu$ m per pixel. The time between two pulses ( $\Delta t$ ) was fixed to 220  $\mu$ s, in order to record a 10-pixel displacement between the pulses at the lowest flow rate. A total of 1000 images were recorded for each condition.

In the vicinity of the flame, the particle concentration is estimated to 0.005 particle per pixel. Such a low concentration is caused by the difficulties of effectively seeding the flow, as the oxygen flow rate had to be split between the ozone generators and the atomizer. For conventional PIV, this very low concentration requires a minimum interrogation window size (IWS) of 32 x 32 pixels (0.64 x 0.64 mm<sup>2</sup>), which leads in our conditions to an insufficient spatial resolution for accurate measurements. To tackle this difficulty, a more advanced and

adapted post-processing approach has been specifically developed at the CORIA laboratory, and is detailed below.

## **2.2. Particle Image Velocimetry (PIV) images post-processing**

Before applying the PIV image processing, an advanced background correction is performed from conditioned averaged images, one at  $t$  and one at  $t + \Delta t$ . A standard background correction is not adapted in the case of low-densities due to the difficulty to remove the individual particle signal on averaged images, even when 1000 images are considered. In our approach, the conditioned background images are then obtained by averaging all the instantaneous images but without integrating the signal of particles in the process using a Kuwahara filter. This specific image processing improves the estimation of background images in particular in low density regions. Following the background correction, only the particle signal remains on the corrected images. Then, the spatial calibration is done with a well-defined target (0.977 x 0.977 mm), and is used to estimate a polynomial camera model of 3<sup>rd</sup> order used to dewarp each image, ensuring a perfect alignment of both wall and burner axes within the (x, y) frame. This step also corrects any image distortion induced by the camera lens. From this step, PIV processing starts by an extraction of the particles position in the images using a 2D correlation pattern recognizing technique. Between 1500 and 3500 particles are detected on each image, depending on the experimental conditions. The vector calculation is then initiated at the particle location, and not on a regular mesh as it is usually performed when the particles density is higher. This calculation is based on an iterative continuous window shift technique [25,26], starting with an interrogation window size (IWS) of 64 x 64, and reaching an IWS of 8 x 8 pixels (0.16 x 0.16 mm<sup>2</sup>) in the final pass. This results in a series of non-regular velocity fields which are validated with a rate higher than 85%. The scaling in the real coordinated system is realized with the burner plate as reference, with an accuracy of  $\pm 20 \mu\text{m}$ . The final step consists in computing a mean velocity field on a regular mesh by averaging every



instantaneous vector in small cells at each mesh node, the cell size being compatible with the PIV resolution of  $8 \times 8$  pixels. This processing method allows a significant improvement in the particle detection in the area close to the flame front. A comparison of the axial velocity profiles determined using a conventional image processing method, i.e., with an IWS of  $32 \times 32$  pixels, and the present one is presented in Figure S1 of the Supplementary Material.

Axial velocity profiles are finally extracted from the mean velocity field by averaging on a radial width of  $\pm 1$  mm around the centre of the burner. A two-dimensional velocity field in reactive conditions is shown in Figure 2. It demonstrates that the radial ( $u_r$ ) distribution of the velocities is axisymmetric, and that the axial velocity ( $u_a$ ) profile at the burner exit is almost uniform over the entire diameter of the burner (10 mm). The flat cool flame front, stabilized two millimetres under the heated plate, can be distinguished on the axial velocity profile. This confirms the efficiency of the converging nozzle geometry, and constitutes further justification of the averaging process over a region of  $\pm 1$  mm used in the image post-processing, as the axial velocity can be considered constant over a significant portion of the burner diameter. From Root Mean Square (RMS) analysis, the uncertainty on the determination of the axial velocity with the PIV technique is estimated to be  $\pm 5\%$ . This lead to an uncertainty in the flame speed determination lying between  $0.83$  and  $1.05 \text{ cm.s}^{-1}$ , depending on the value of the reference axial velocity  $S_{u,\text{ref}}$  (minimum velocity upstream of the flame front, as shown in Figure 3), which has been averaged at  $\pm 1 \text{ cm.s}^{-1}$ .

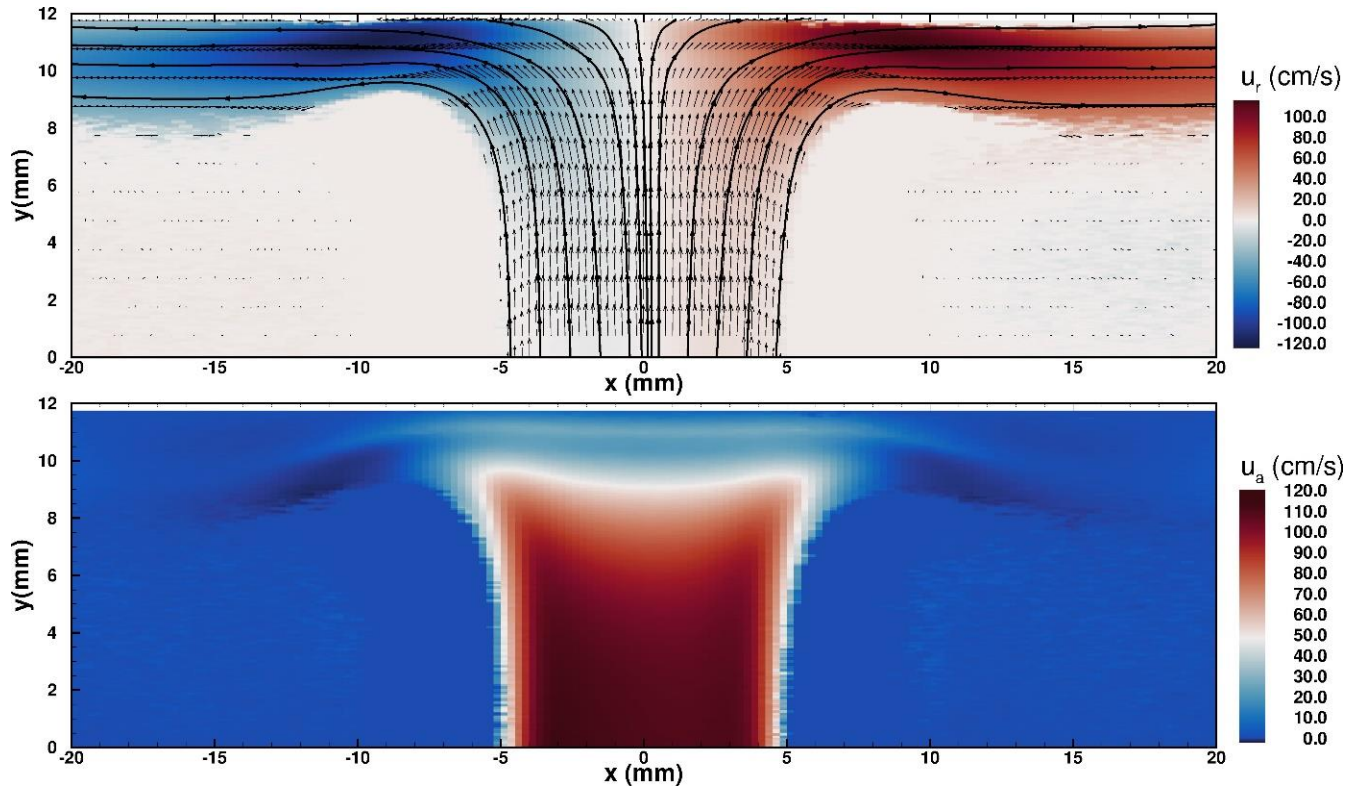


**Figure 2.** Radial velocity streamlines (top) and axial velocity profile (bottom) of a DME/O<sub>2</sub>/O<sub>3</sub> cool flame at  $\phi = 0.4$  and  $x_{O_3} = 1.9\%$ .  $u_r$  represents the radial velocity,  $u_a$  the axial velocity,  $y$  the Height Above the Burner (HAB) and  $x$  the burner radius.

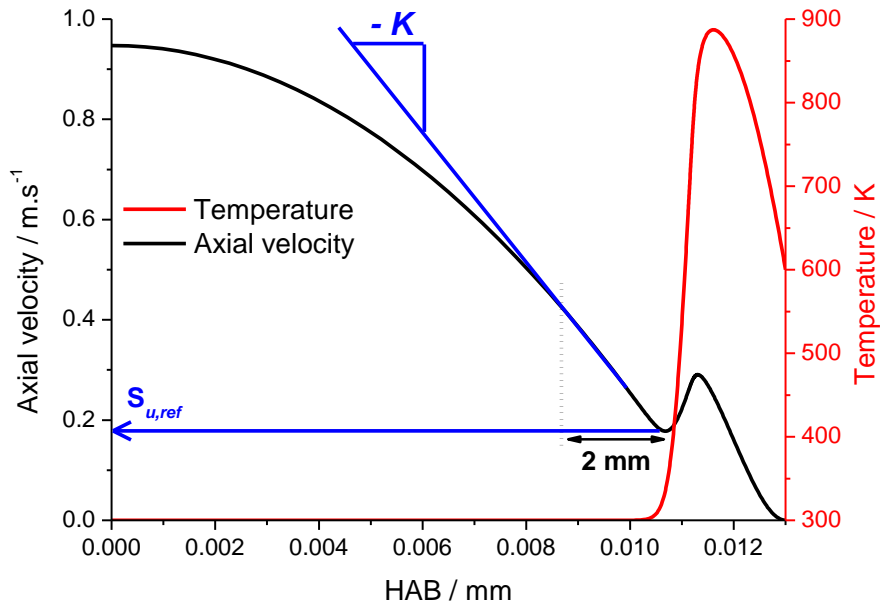


**Figure 3.** Simulated temperature (red) and axial velocity (black) profiles of a cool flame. Determination of the couple ( $S_{u,ref}$ ,  $K$ ) is also shown.

### 2.3. Flame conditions

Five stable cool flame conditions were selected for the measurement of cool flame speeds, and are summarized in Table 1. Note that the inlet velocity ( $u_{in}$ ) range is limited as it is constrained by the stability domain of the cool flames, which is known to be narrower than for hot flames. Furthermore, at high inlet velocity (and strain rate, usually calculated as the ratio between the flow velocity and the burner/plate distance), the cool flames tend to stabilize closer to the stagnation plate, leading to difficulties in resolving the entire velocity profile. On the contrary, at low inlet velocity, the particle seeding is not sufficient to provide accurate measurement of the velocity field in the burner.

The detailed flames conditions are provided in the Supplementary Material (Table T1).

$\phi$	$x_{O_3}^* / \%$	$u_{in} / \text{cm.s}^{-1}$
0.5	1.5	65 – 80
0.45	1.7	75 – 110
0.4	1.7	65 – 85
0.4	1.9	75 – 110
0.3	2.0	65 – 95

\*The indicated values correspond to the ozone mole fraction in the DME/O<sub>2</sub>/O<sub>3</sub> mixture

**Table 1.** Experimental conditions for the investigated DME/O<sub>2</sub>/O<sub>3</sub> cool flames.

### 2.4. Flame simulations

The axial velocity profiles for all flames conditions were simulated with multicomponent transport using the Pre-Mixed Burner Stagnation Flame module of Chemkin-Pro 2021 [27]. The size of the simulation domain (see Table T1 in Supplementary Material) was varied depending on the studied conditions, as detailed later. The GRAD and CURV parameters were fixed at 0.03 each, resulting in ~ 450 points per simulation, which is sufficient

to ensure accurate simulations of the reference axial velocity  $S_{u,ref}$  within a 1% uncertainty, as demonstrated in the Supplementary Material (Figure S2). The Soret effect option was disabled for the axial velocity profiles simulations as it did not significantly modify the reference axial velocity and allowed a drastic reduction of the computational time. The energy equation was solved for simulation; hence the experimental temperature profile was not used as an input. The experimental and simulated temperature profiles of lean DME/O<sub>2</sub>/O<sub>3</sub> cool flames were compared in our previous study [23] and showed an excellent agreement.

A detailed kinetic mechanism recently developed in our group [23] has been used, it is based on the AramcoMech1.3 mechanism [28] with reassessed reaction pathways and modified Arrhenius parameters. It was validated on the prediction of the mole fraction profiles of intermediates species above the burner for DME/O<sub>2</sub>/O<sub>3</sub> cool flames. Three different O<sub>3</sub>-submechanisms from the literature, respectively from Jian et al. [20], Zhao et al. [21] and Halter et al. [22], were coupled to the aforementioned mechanism [23]. A summary of the different reactions and their associated modified Arrhenius reaction rate coefficients is given in the Table T2 of the Supplementary Material. Note that these three O<sub>3</sub>-submechanisms have been very recently [20] compared to experimental data on O<sub>3</sub> decomposition, O<sub>3</sub>/O<sub>2</sub> flame speeds and H<sub>2</sub>/O<sub>2</sub>/O<sub>3</sub> reaction in a flow reactor, showing satisfactory predictions in these experimental conditions.

### 3. RESULTS AND DISCUSSION

#### 3.1. Axial velocity profiles

The axial velocity profile measured for the strained cool flame at  $\phi = 0.5$ ,  $x_{O_3} = 1.5\%$  is pictured for five different inlet velocities  $u_{in}$  (and strain rates) as an example of the obtained results in Figure 4. The increase of velocity upstream of the flame front due to thermal expansion is less pronounced than in hot flame cases since the heat release of cool flames is

significantly lower. The entire velocity profile is well defined in each condition supporting the use of silicon oil droplets and the applied PIV image processing. As the inlet velocity (and strain rate) increases, the flame moves towards the stagnation plate and the acceleration observed in the flame front is reduced in accordance with a decrease of the maximum flame temperature.

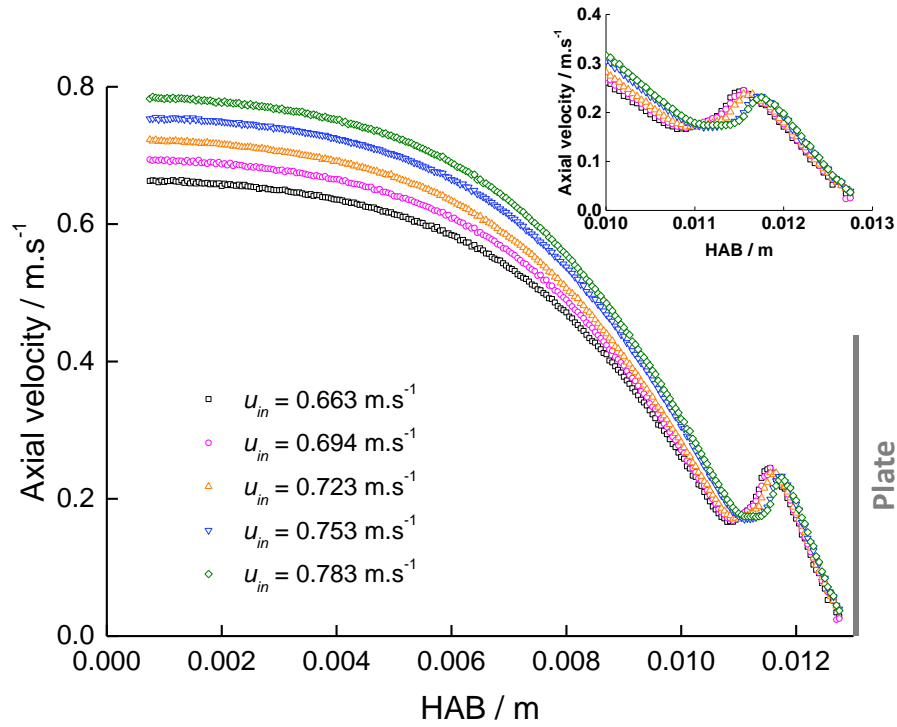


**Figure 4.** Axial velocity profiles as a function of the Height Above the Burner (HAB) of a DME/O<sub>2</sub>/O<sub>3</sub> cool flame at  $\phi = 0.5$ ,  $x_{O_3} = 1.5\%$ , for five different inlet velocities  $u_{in}$ .

The measured axial velocity profiles in the strained cool flames were compared with simulations performed with the Pre-Mixed Burner Stagnation Flame module of Chemkin-Pro, following the methodology proposed in [29–31]. It consists in imposing the exact boundary conditions inferred from the PIV experiments, as it is recognized that the experimental flow field in stagnation plate burner configuration is usually neither a plug flow nor a potential flow [32] and that 1D approaches typically fail in providing accurate prediction of the corresponding velocity profile [33]. In this work, the inlet position of the simulation domain was fixed two millimetres before the minimum velocity upstream of the flame front position (defined as  $S_{u,ref}$ ).

Experimental strain rates  $K$  and inlet velocities were inferred from the axial velocity profile 2 mm upstream from  $S_{u,ref}$ , as pictured in Figure 3. The effect of the domain size on the accuracy of the velocity profile, targeting both the reference velocity  $S_{u,ref}$  and its position above the burner, was studied and the results are pictured in Figures S3 and S4 of the Supplementary Material. Results showed that the simulated  $S_{u,ref}$  were similar within 1% for domain sizes below 8 mm, but that selecting a too small domain size, here less than 3.2 mm, led to a greater deviation. The computational domain length therefore lies between 3.05 and 4.45 mm, depending on the flame conditions. To ensure reproducible determination of the experimental  $K$ , the experimental axial velocity profile was fitted using a 2<sup>nd</sup>-order polynomial function beforehand.

The axial velocity profiles simulated using the three aforementioned ozone-submechanisms [20–22] were compared to the experimental ones. Two flame conditions at  $\phi = 0.5$ ,  $x_{O_3} = 1.5\%$  and  $\phi = 0.3$ ,  $x_{O_3} = 2.0\%$  are presented in Figure 5 and Figure 6 respectively. For the sake of brevity, the same comparisons for other flame conditions are presented in Figures S5 to S7 in the Supplementary Material, and the exact boundary conditions used for the simulation are given in the Table T1 of the Supplementary Material. Comparing the three different  $O_3$ -submechanisms, large variations in the prediction of the velocity profile can be observed between the Halter et al. model and the two other models, with an important underprediction of the minimum velocity  $S_{u,ref}$  for the Halter et al. model. It should be noted that in the case  $\phi = 0.3$ ,  $x_{O_3} = 2\%$  (Figure 6), the Halter et al. model predicts almost no minimum velocity for higher strain rates, but only an inflection of the axial velocity curve upstream of the flame front. The predictions from the Jian et al. and Zhao et al. models are comparable, as both models accurately describe the overall velocity profile.

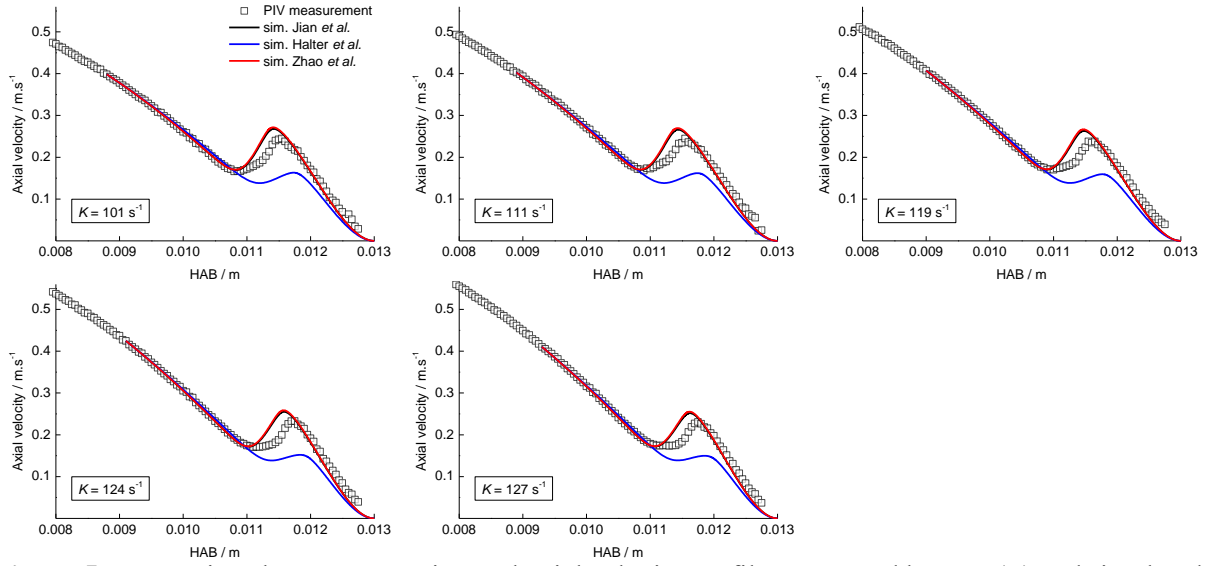


**Figure 5.** Comparison between experimental axial velocity profiles measured by PIV ( $\square$ ) and simulated ones with different  $O_3$ -submechanisms, respectively from Jian et al., Halter et al. and Zhao et al., for the cool flame at  $\phi = 0.5$ ,  $x_{O_3} = 1.5\%$ , at different strain rates.

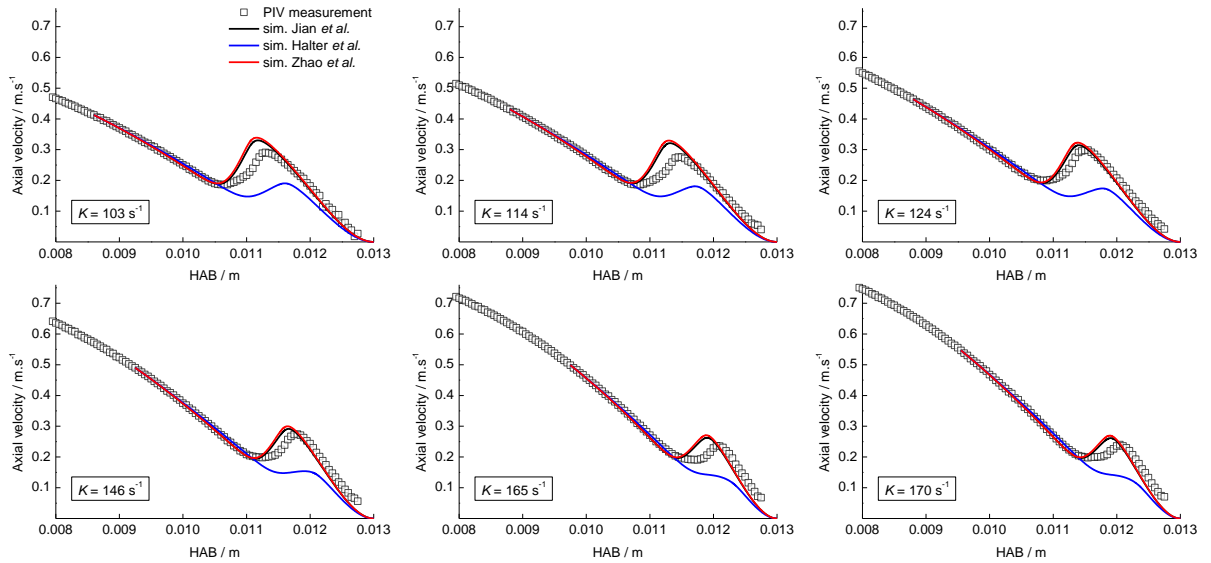


**Figure 6.** Comparison between experimental axial velocity profiles measured by PIV ( $\square$ ) and simulated ones with different  $O_3$ -submechanisms, respectively from Jian et al., Halter et al. and Zhao et al., for the cool flame at  $\phi = 0.3$ ,  $x_{O_3} = 2.0\%$ , at different strain rates.

In order to evaluate the capabilities of these models to predict cool flame speeds, the Root-Mean-Square Error (RMSE) between experimental and simulated  $S_{u,ref}$  was calculated over the investigated strain rate range, for the five flames conditions.

The RMSE data are summed up in the Table 2, for each O<sub>3</sub>-submechanism. One can see that the Halter et al. submechanism constantly underestimates the value of S<sub>u,ref</sub>, while the two other models yield similar performance.

Condition	Root-Mean-Square Error (RMSE)		
	Jian et al.	Halter et al.	Zhao et al.
$\phi = 0.3, x_{O_3} = 2.0\%$	0.5	4.7	0.5
$\phi = 0.4, x_{O_3} = 1.9\%$	1.2	5.9	0.7
$\phi = 0.4, x_{O_3} = 1.7\%$	0.2	3.8	0.3
$\phi = 0.45, x_{O_3} = 1.7\%$	0.2	4.5	0.4
$\phi = 0.5, x_{O_3} = 1.5\%$	0.2	3.1	0.2

**Table 2.** Root Mean-Square Error (RMSE) calculated for each flame condition with the different O<sub>3</sub>-submechanisms

A possible explanation for the constant underestimation of the flame speed by the model of Halter et al. is the definition of the ozone decomposition within the model, where only N<sub>2</sub>, O<sub>2</sub> and O<sub>3</sub> are declared as collision partners in the  $O_3 + M \rightleftharpoons O_2 + \ddot{O} + M$  reaction, in contrast with the other two mechanisms (for which all species are considered with a collision efficiency of 1, except if specified). In our experimental conditions, the fuel mole fraction lies between 10 and 15% of the mixture. The absence of DME as a third-body in the ozone decomposition reaction can therefore lead to a lowered reactivity of the Halter et al. model (see Table T2 in the Supplementary Material). This aspect has been tested by replacing the O<sub>3</sub>+M decomposition reactions of the model of Jian et al. by the O<sub>3</sub>+M reactions of Halter et al., showing a deterioration in the prediction of the axial velocity profile, as seen in Figure S8 in the Supplementary Material.

For the following sections, the Jian et al. submechanism will be used solely, because of its more recent rate constants data and its good performance in predicting S<sub>u,ref</sub>.



### 3.2. Determination of the unstrained cool flame speed $S_{u,0}$

A well-established method [34] has been widely used to derive the unstrained flame speed  $S_{u,0}$  of hot flames. It consists of measuring the axial velocity profiles for different strain rates ( $K$ ) and determining the reference velocity ( $S_{u,ref}$ ) as represented in Figure 3. From the plot of  $S_{u,ref} = f(K)$ , the extrapolation to strain rate  $K = 0$  returns the unstrained laminar flame speed  $S_{u,0}$ .

Both linear [35] and non-linear [36] extrapolation methods have been used in the past. Vagelopoulos et al. [34] and Chong and Hochgreb [37] have demonstrated that for low-strain rate hot flames ( $50 - 250 \text{ s}^{-1}$ ), the linear extrapolation method yields accurate results within a reported uncertainty of  $\sim 1\text{-}2 \text{ cm.s}^{-1}$ . In the case of cool flames, for which the speed is significantly smaller, this added uncertainty might however be problematic. The issue of non-linear extrapolation was revisited by Egolfopoulos et al. [38–41] with a computational approach, where the simulated  $S_{u,ref}$  at various  $K$  (using a counter-flow flame code) and the simulated  $S_{u,0}$  at  $K = 0$  (using the freely propagating flame module of the PREMIX code) are fitted using a polynomial function. This computed curve is vertically translated to best fit the experimental data and the experimental flame speeds are derived from this non-linear extrapolation [40]. This method however requires using a kinetic mechanism that yields an accurate value of  $S_{u,0}$ .

In the present work, a similar approach has been applied but without using the  $S_{u,0}$  calculated from a freely-propagating flame module. Axial velocity profiles were simulated using the Pre-Mixed Burner Stagnation Flame module of Chemkin-Pro by progressively decreasing the strain rate, from which a numerical curve  $S_{u,ref} = f(K)$  was extracted, as shown in Figure 7. The simulated curve  $S_{u,ref} = f(K)$  is then fitted using a 2<sup>nd</sup> order polynomial and vertically translated to best fit the experimental results [37-40]. The experimental unstrained cool flame speed  $S_{u,0}$  is then considered at  $K = 0$ . Figure 7 shows the application of this method

for the five DME/O<sub>2</sub>/O<sub>3</sub> cool flames conditions. As seen in Figure 7, the numerical and experimental  $S_{u,0}$  lie very close to each other (those values are given in Table 3 for the five flames studied, columns 2 and 3).

Limitations of this method should however be considered. First, unlike hot flames, the fuel conversion is only partial in a cool flame. Therefore, thermochemical equilibrium is not reached in the post flame region. This causes non-zero temperature and velocity gradients in the downstream area of the flame. Such results can therefore not be considered as laminar burning velocities, nor modelled using a freely propagating flame module. Secondly, since the stagnation plate temperature (600 K) is below the measured flame peak temperatures of about 900 K [23], such flames are not adiabatic. To assess the effect of this non-adiabaticity on the determined unstrained cool flame speeds  $S_{u,0}$ , additional simulations were carried out. The stagnation plate module of Cantera 2.6 [42] was used in the same domain width and input compositions as in the simulations of Figures 5-6, and the stagnation plate temperature was progressively increased until it reached a temperature identical to the maximal flame temperature within a 0.01% tolerance. The strain rate was varied, and the  $S_{u,ref} = f(K)$  results were fitted to a 2<sup>nd</sup> order polynomial leading to  $S_{u,0}$  values at  $K=0$  reported in Figure 8 and Table 3 (column 4). Because these cool flames are below 1000 K and sufficiently lifted to neglect heat losses to the exit burner nozzle, they can be considered adiabatic, as for example in the well-known heat flux method [43]. The adiabatic  $S_{u,0}$  results (Table 3) are identical within the uncertainty of the experiments to the simulated values at a plate temperature of 600 K, demonstrating a negligible effect of the plate temperature on the measured unstrained cool flame velocities.

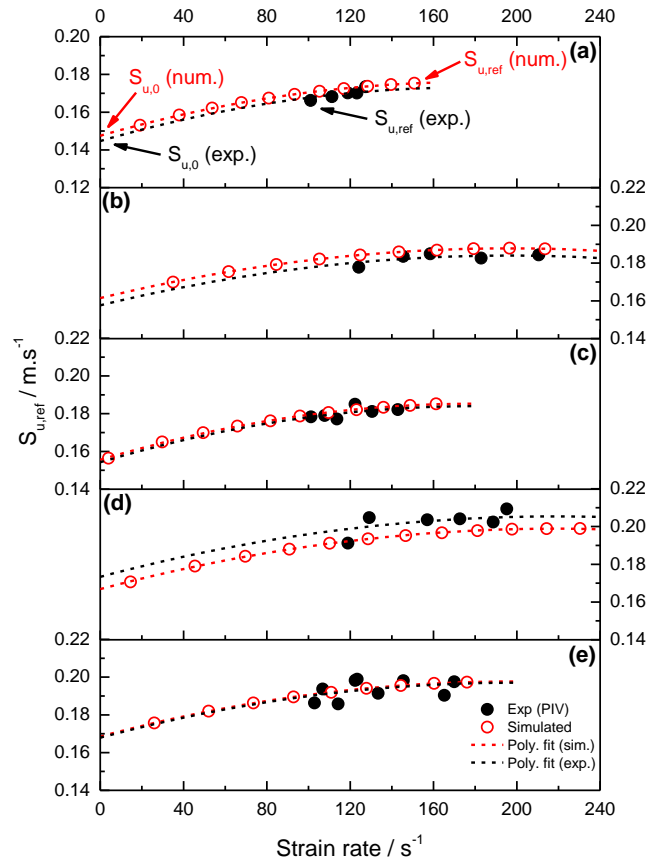


**Figure 7.** Variations of  $S_{u,ref}$  with  $K$  and determination of  $S_{u,0}$  using a numerically assisted non-linear extrapolation. Flame conditions:  $\phi = 0.5$ ,  $x_{O_3} = 1.5\%$  (a),  $\phi = 0.45$ ,  $x_{O_3} = 1.7\%$  (b),  $\phi = 0.4$ ,  $x_{O_3} = 1.7\%$  (c),  $\phi = 0.4$ ,  $x_{O_3} = 1.9\%$  (d) and  $\phi = 0.3$ ,  $x_{O_3} = 2.0\%$  (e).

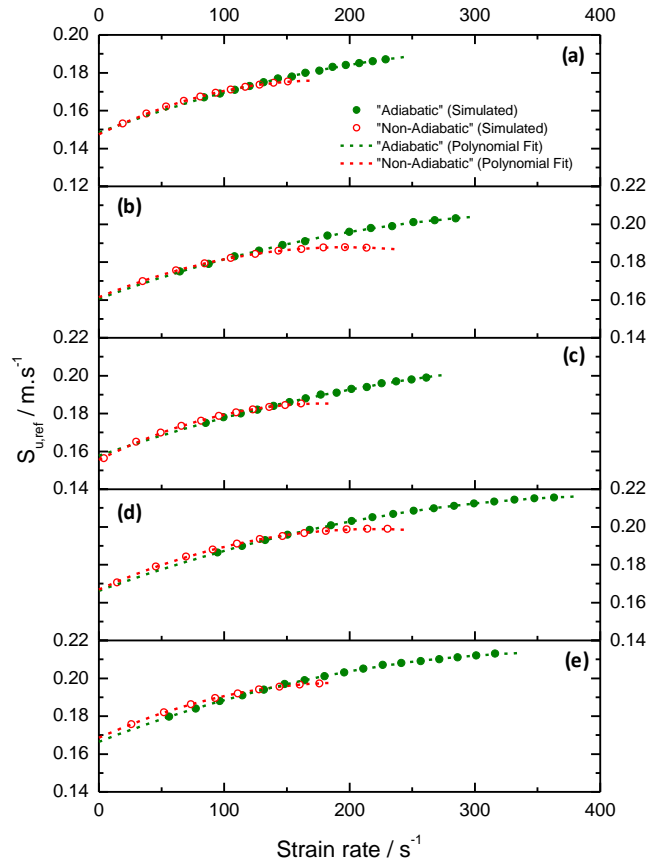


**Figure 8.** Simulated variations of  $S_{u,ref}$  with  $K$  using a non-linear extrapolation in adiabatic and non-adiabatic conditions. Flames conditions:  $\phi = 0.5$ ,  $x_{O_3} = 1.5\%$  (a),  $\phi = 0.45$ ,  $x_{O_3} = 1.7\%$  (b),  $\phi = 0.4$ ,  $x_{O_3} = 1.7\%$  (c),  $\phi = 0.4$ ,  $x_{O_3} = 1.9\%$  (d) and  $\phi = 0.3$ ,  $x_{O_3} = 2.0\%$  (e).

Flame conditions	$S_{u,0} / \text{cm.s}^{-1}$		
	Experimental	Simulated	Simulated Adiabatic
$\phi = 0.5$ , $x_{O_3} = 1.5\%$	$14.5 \pm 1 \text{ cm.s}^{-1}$	14.7	14.8
$\phi = 0.45$ , $x_{O_3} = 1.7\%$	15.8	16.1	16.1
$\phi = 0.4$ , $x_{O_3} = 1.7\%$	15.4	15.6	15.8
$\phi = 0.4$ , $x_{O_3} = 1.9\%$	17.3	16.7	16.6
$\phi = 0.3$ , $x_{O_3} = 2.0\%$	16.8	16.9	16.6

**Table 3.** Experimental and simulated unstrained cool flame speeds  $S_{u,0}$  for all the cool flames conditions.

By comparing both flames at  $x_{O_3} = 1.7\%$ , one can see that the cool flame speed increases moderately as the equivalence ratio increases from 0.4 to 0.45. This effect is captured by the simulation. A comparison of both flames at  $\phi = 0.4$  ( $x_{O_3} = 1.7\%$  and  $1.9\%$ ) demonstrates the

important effect of ozone addition on the cool flame speed, which increases by about  $2 \text{ cm.s}^{-1}$  (experimentally) when the ozone mole fraction increases only from 1.7% to 1.9%. This effect is also captured in the simulation, yet underestimated.

### 3.3. Kinetic analysis

A brute-force sensitivity analysis was performed on the experimental reference axial velocity  $S_{u,\text{ref}}$ , using the Jian et al.  $\text{O}_3$ -submechanism [20] in conjunction with our previously published DME sub-mechanism [23], with the stagnation flame module of the Cantera 2.6 solver [42]. To do so, the domain size and input conditions were chosen as in the experiments and simulations of Figures 5-6, and the sensitivity coefficients of the reactions on the minimum of axial velocity associated with the cool flame were evaluated from a positive and negative variation of the frequency factor of each reaction by 5%. A positive sensitivity coefficient therefore means that increasing the reaction rate constant for the associated reaction increases the reference cool flame velocity  $S_{u,\text{ref}}$ , and vice versa. The two most extreme conditions were selected for the sensitivity analyses, respectively the flame at  $\phi = 0.3$ ,  $x_{\text{O}_3} = 2.0\%$ , which contains the highest ozone mole fraction in this study, and the flame at  $\phi = 0.5$ ,  $x_{\text{O}_3} = 1.5\%$ , which contains the lowest. The results are displayed for the 16 reactions with the highest absolute sensitivity coefficients in Figure 9.

In both conditions, it is observed that the simulated  $S_{u,\text{ref}}$  is strongly dependent on the branching between the decomposition of the  $\dot{\text{Q}}\text{OOH}$  into two molecules of formaldehyde and an  $\dot{\text{O}}\text{H}$  radical, which tends to decrease the cool flame velocity, and the addition of  $\dot{\text{Q}}\text{OOH}$  to  $\text{O}_2$ , which will lead to indirect chain-branching. Among the other important features is the competition between the  $\text{RO}\dot{\text{O}} \rightleftharpoons \dot{\text{Q}}\text{OOH}$  pathway, and the  $2 \text{RO}\dot{\text{O}} \rightleftharpoons 2 \text{R}\dot{\text{O}} + \text{O}_2$  route. The latter is traditionally associated with atmospheric conditions, but was previously observed to be

significant in our conditions [23]. To a more reduced extent, the branching of  $\dot{R}$  radical between addition to  $O_2$  or direct scission into formaldehyde and a methyl radical is also of importance. One can however note the large sensitivity coefficient of the H-atom abstraction reaction on DME by  $\dot{O}H$ . A striking feature of these results is that, in contrast with hot flames burning velocities, the most sensitive reactions are all directly part of the fuel submechanism, the  $O_3 + M \rightleftharpoons O_2 + \ddot{O} + M$  reaction only ranking as the fourth most sensitive reaction. This is a strong argument in favour of these experimental data as potential targets for the validation of kinetic models in the low-temperature domain.

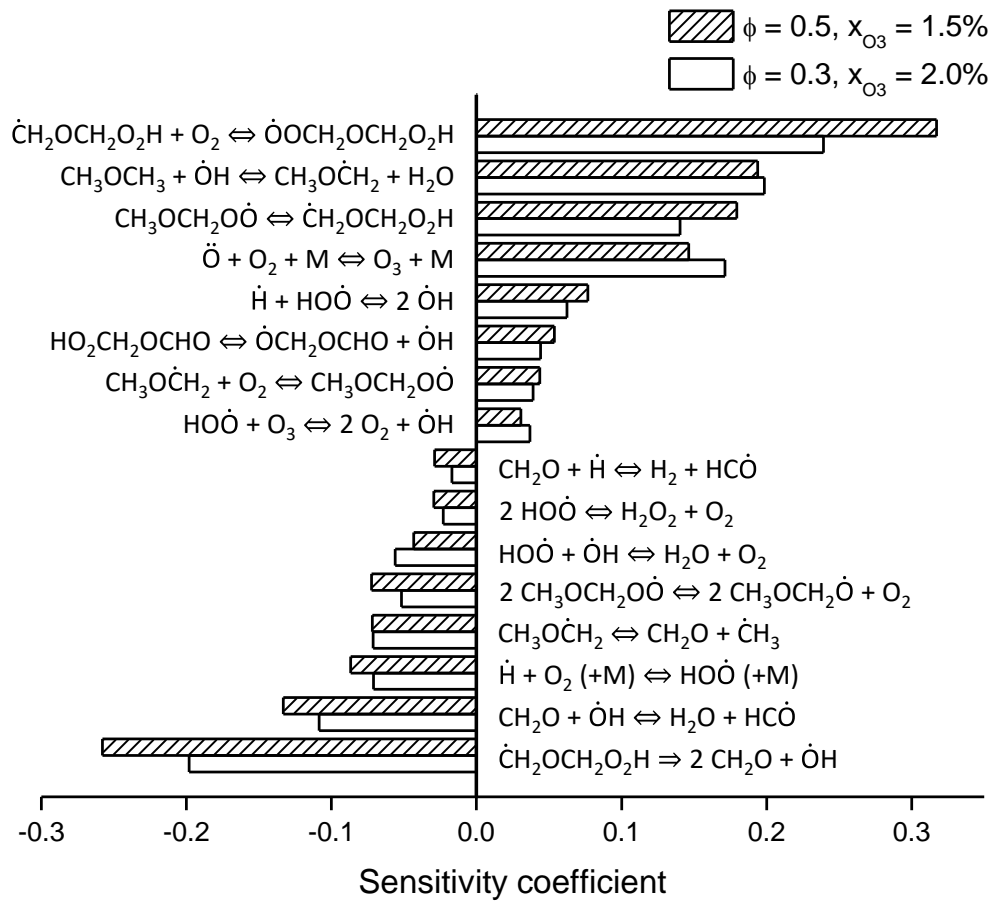


**Figure 9.** Brute-force sensitivity analysis performed on the reference cool flame  $S_{u,ref}$ , at  $\phi = 0.5$ ,  $x_{O_3} = 1.5\%$  and at  $\phi = 0.3$ ,  $x_{O_3} = 2.0\%$ .

#### 4. CONCLUSIONS

The measurement of ozone-seeded dimethyl ether cool flame speeds was successfully realized in a stagnation plate burner for the first time. The PIV technique was used to measure the 2-D velocity profiles, from which axial velocity profiles were inferred to measure the unstrained cool flame speeds. For this purpose, an in-house PIV image processing method has been developed and used in order to improve the accuracy of the measurement. Five flame conditions, with equivalence ratios varying from 0.3 to 0.5 and ozone mole fraction varying from 1.5 to 2% were used to compare experimental results with kinetic modeling. Three ozone-submechanisms, namely from Jian et al., Zhao et al. and Halter et al., were coupled with our previous mechanism validated in DME/O<sub>2</sub>/O<sub>3</sub> cool flames and used to compare experimental and simulated axial velocity profiles, emphasizing the importance of the choice of the O<sub>3</sub>-submechanism. The Jian et al. submechanism was selected because of its good predictive ability for axial velocity profiles and was used to determine the unstrained cool flame speed  $S_{u,0}$  for each tested condition. A numerical assisted non-linear extrapolation method is proposed for the determination of  $S_{u,0}$ . Additionally, simulations for which the plate temperature reaches the maximal flame temperature (i.e., adiabatic conditions) were performed, demonstrating a negligible effect of the plate temperature on the unstrained cool flame velocity. However, for the purpose of mechanism validation, the direct comparison with the experimental axial velocity profiles should be preferred as it requires no numerical assisted method. Values of  $S_{u,0}$  were found to lie between ~14 and 17 cm.s<sup>-1</sup> within the range of flame conditions studied here, showing a limited effect of the equivalence ratio variations, and a more striking effect of the ozone concentration. Finally, sensitivity analyses performed on the reference axial velocity  $S_{u,ref}$  in two flame conditions emphasize the importance of the fuel low-temperature chain-branching pathways, over the ozone submechanism.

## **Acknowledgements**

This work is a contribution to the LabEx CaPPA project funded by the French National Agency under contract « ANR-11-LABX-0005-01 », the CPER research project CLIMIBIO funded by the French Ministère de l'Enseignement Supérieur et de la Recherche and the MéOL (Métrologie Optique de Lille) platform. The authors thank the Regional Council « Hauts-de-France » and the « European Regional Development Fund » for their financial support to these projects.

## **Supplementary material**

Supplementary Material can be found in the attached file.

## **Authors contributions**

Conceptualization: **L. Pillier, G. Vanhove**; Data curation: **All authors**; Formal analysis: **T. Panaget, B. Lecordier, Y. Fenard, G. Vanhove, L. Pillier, P. Bragança, C. Cuvier**; Funding acquisition: **L. Pillier, G. Vanhove**; Investigation: **T. Panaget, P. Bragança, L. Pillier, C. Cuvier**; Methodology: **All authors**; Project administration: **L. Pillier, G. Vanhove**; Resources: **L. Pillier, G. Vanhove, B. Lecordier, C. Cuvier**; Software: **T. Panaget, Y. Fenard, G. Vanhove, B. Lecordier, P. Bragança, C. Cuvier**; Supervision: **L. Pillier, G. Vanhove, Y. Fenard**; Validation: **All authors**; Visualization: **All authors**; Roles/Writing - original draft: **T. Panaget, L. Pillier, G. Vanhove**; and Writing - review & editing: **All authors**



## REFERENCES

- [1] Davy H. VIII. Some new experiments and observations on the combustion of gaseous mixtures, with an account of a method of preserving a continued light in mixtures of inflammable gases and air without flame. *Philos Trans R Soc Lond* 1817;107:77–85. <https://doi.org/10.1098/rstl.1817.0009>.
- [2] Nayagam V, Dietrich DL, Ferkul PV, Hicks MC, Williams FA. Can cool flames support quasi-steady alkane droplet burning? *Combust Flame* 2012;159:3583–8. <https://doi.org/10.1016/j.combustflame.2012.07.012>.
- [3] Ju Y. Understanding cool flames and warm flames. *Proc Combust Inst* 2021; 38: 83 - 119. <https://doi.org/10.1016/j.proci.2020.09.019>
- [4] Ju Y, Reuter C, Yehia OR, Farouk TI, Won SH. Dynamics of cool flame. *Progress in Energy and Combustion Science* 2019; 75:100787. <https://doi.org/10.1016/j.pecs.2019.100787>
- [5] Bhagatwala A, Chen JH, Lu T. Direct numerical simulations of HCCI/SACI with ethanol. *Combust Flame* 2014;161:1826–41. <https://doi.org/10.1016/j.combustflame.2013.12.027>.
- [6] Ju Y, Reuter CB, Won SH. Numerical simulations of premixed cool flames of dimethyl ether/oxygen mixtures. *Combust Flame* 2015;162:3580–8. <https://doi.org/10.1016/j.combustflame.2015.06.014>.
- [7] Ju Y. On the propagation limits and speeds of premixed cool flames at elevated pressures. *Combust Flame* 2017;178:61–9. <https://doi.org/10.1016/j.combustflame.2017.01.006>.
- [8] Zhao P, Liang W, Deng S, Law CK. Initiation and propagation of laminar premixed cool flames. *Fuel* 2016;166:477–87. <https://doi.org/10.1016/j.fuel.2015.11.025>.
- [9] Gao X, Zhang Y, Adusumilli S, Seitzman J, Sun W, Ombrello T, et al. The effect of ozone addition on laminar flame speed. *Combust Flame* 2015;162:3914–24. <https://doi.org/10.1016/j.combustflame.2015.07.028>.
- [10] Ombrello T, Won SH, Ju Y, Williams S. Flame propagation enhancement by plasma excitation of oxygen. Part I: Effects of O<sub>3</sub>. *Combust Flame* 2010;157:1906–15. <https://doi.org/10.1016/j.combustflame.2010.02.005>.
- [11] Foster M, Pearlman H. Cool Flame Propagation Speeds. *Combust Sci Technol* 2007;179:1349–60. <https://doi.org/10.1080/00102200601147864>.
- [12] Brown MQ, Belmont EL. Effects of ozone on n-heptane low temperature chemistry and premixed cool flames. *Combust Flame* 2021;225:20–30. <https://doi.org/10.1016/j.combustflame.2020.10.029>.
- [13] Hajilou M, Brown MQ, Brown MC, Belmont E. Investigation of the structure and propagation speeds of n-heptane cool flames. *Combust Flame* 2019;208:99–109. <https://doi.org/10.1016/j.combustflame.2019.06.020>.
- [14] Hajilou M, Belmont E. Characterization of ozone-enhanced propane cool flames at sub-atmospheric pressures. *Combust Flame* 2018;196:416–23. <https://doi.org/10.1016/j.combustflame.2018.07.001>.
- [15] Hajilou M, Ombrello T, Won SH, Belmont E. Experimental and numerical characterization of freely propagating ozone-activated dimethyl ether cool flames. *Combust Flame* 2017;176:326–33. <https://doi.org/10.1016/j.combustflame.2016.11.005>.
- [16] Belmont E, Ombrello T, Brown M, Carter C, Ellzey J. Experimental and numerical investigation of freely propagating flames stabilized on a Hencken Burner. *Combust Flame* 2015;162:2679–85. <https://doi.org/10.1016/j.combustflame.2015.03.025>.
- [17] Ombrello T, Carter C, Katta V. Burner platform for sub-atmospheric pressure flame studies. *Combust Flame* 2012;159:2363–73. <https://doi.org/10.1016/j.combustflame.2012.03.010>.

- [18] Reuter CB, Won SH, Ju Y. Cool Flames Activated by Ozone Addition. 53rd AIAA Aerosp. Sci. Meet., Kissimmee, Florida: American Institute of Aeronautics and Astronautics; 2015. <https://doi.org/10.2514/6.2015-1387>.
- [19] Liao H, Kang S, Hansen N, Zhang F, Yang B. Influence of ozone addition on the low-temperature oxidation of dimethyl ether in a jet-stirred reactor. *Combust Flame* 2020;214:277–86. <https://doi.org/10.1016/j.combustflame.2019.12.036>.
- [20] Jian J, Hashemi H, Wu H, Jasper AW, Glarborg P. A reaction mechanism for ozone dissociation and reaction with hydrogen at elevated temperature. *Fuel* 2022;322:124138. <https://doi.org/10.1016/j.fuel.2022.124138>.
- [21] Zhao H, Yang X, Ju Y. Kinetic studies of ozone assisted low temperature oxidation of dimethyl ether in a flow reactor using molecular-beam mass spectrometry. *Combust Flame* 2016;173:187–94. <https://doi.org/10.1016/j.combustflame.2016.08.008>.
- [22] Halter F, Higelin P, Dagaut P. Experimental and Detailed Kinetic Modeling Study of the Effect of Ozone on the Combustion of Methane. *Energy Fuels* 2011;25:2909–16. <https://doi.org/10.1021/ef200550m>.
- [23] Panaget T, Mokrani N, Batut S, Lahccen A, Fenard Y, Pillier L, et al. Insight into the Ozone-Assisted Low-Temperature Combustion of Dimethyl Ether by Means of Stabilized Cool Flames. *J Phys Chem A* 2021;125:9167–79. <https://doi.org/10.1021/acs.jpca.1c05583>.
- [24] Kähler C, Sammler B, Kompenhans J. Generation and control of tracer particles for optical flow investigations in air. *Exp Fluids* 2002;33:736–42. <https://doi.org/10.1007/s00348-002-0492-x>.
- [25] Lecordier B, Demare D, Vervisch LMJ, Réveillon J, Trinite M. Estimation of the accuracy of PIV treatments for turbulent flow studies by direct numerical simulation of multi-phase flow. *Meas Sci Technol* 2001;12:1382.
- [26] Balusamy S, Cessou A, Lecordier B. Direct measurement of local instantaneous laminar burning velocity by a new PIV algorithm. *Exp Fluids* 2011;50:1109–21. <https://doi.org/10.1007/s00348-010-1027-5>.
- [27] Ansys Chemkin Pro, Release 2021 R1 2021.
- [28] Metcalfe WK, Burke SM, Ahmed SS, Curran HJ. A Hierarchical and Comparative Kinetic Modeling Study of  $C_1 - C_2$  Hydrocarbon and Oxygenated Fuels. *Int J Chem Kinet* 2013;45:638–75. <https://doi.org/10.1002/kin.20802>.
- [29] Durocher A, Meulemans M, Bourque G, Bergthorson JM. Measurements of the laminar flame speed of premixed, hydrogen-air-argon stagnation flames. *Appl Energy Combust Sci* 2021;7:100028. <https://doi.org/10.1016/j.jaecs.2021.100028>.
- [30] Munzar JD, Akih-Kumgeh B, Denman BM, Zia A, Bergthorson JM. An experimental and reduced modeling study of the laminar flame speed of jet fuel surrogate components. *Fuel* 2013;113:586–97. <https://doi.org/10.1016/j.fuel.2013.05.105>.
- [31] Bergthorson JM, Salusbury SD, Dimotakis PE. Experiments and modelling of premixed laminar stagnation flame hydrodynamics. *J Fluid Mech* 2011;681:340–69. <https://doi.org/10.1017/jfm.2011.203>.
- [32] Sung CJ, Kistler JS, Nishioka M, Law CK. Further studies on effects of thermophoresis on seeding particles in LDV measurements of strained flames. *Combust Flame* 1996;105:189–201. [https://doi.org/10.1016/0010-2180\(95\)00189-1](https://doi.org/10.1016/0010-2180(95)00189-1).
- [33] Bouvet N, Davidenko D, Chauveau C, Pillier L, Yoon Y. On the simulation of laminar strained flames in stagnation flows: 1D and 2D approaches versus experiments. *Combust Flame* 2014;161:438–52. <https://doi.org/10.1016/j.combustflame.2013.09.010>.
- [34] Vagelopoulos CM, Egolfopoulos FN. Direct experimental determination of laminar flame speeds. *Symp Int Combust* 1998;27:513–9. [https://doi.org/10.1016/S0082-0784\(98\)80441-4](https://doi.org/10.1016/S0082-0784(98)80441-4).

- [35] Davis SG, Law CK. Determination of and Fuel Structure Effects on Laminar Flame Speeds of C<sub>1</sub> to C<sub>8</sub> Hydrocarbons. *Combust Sci Technol* 1998;140:427–49. <https://doi.org/10.1080/00102209808915781>.
- [36] Tien JH, Matalon M. On the burning velocity of stretched flames. *Combust Flame* 1991;84:238–48. [https://doi.org/10.1016/0010-2180\(91\)90003-T](https://doi.org/10.1016/0010-2180(91)90003-T).
- [37] Chong CT, Hochgreb S. Measurements of laminar flame speeds of acetone/methane/air mixtures. *Combust Flame* 2011;158:490–500. <https://doi.org/10.1016/j.combustflame.2010.09.019>.
- [38] Veloo PS, Wang YL, Egolfopoulos FN, Westbrook CK. A comparative experimental and computational study of methanol, ethanol, and n-butanol flames. *Combust Flame* 2010;157:1989–2004. <https://doi.org/10.1016/j.combustflame.2010.04.001>.
- [39] Ji C, Dames E, Wang YL, Wang H, Egolfopoulos FN. Propagation and extinction of premixed C<sub>5</sub>–C<sub>12</sub> n-alkane flames. *Combust Flame* 2010;157:277–87. <https://doi.org/10.1016/j.combustflame.2009.06.011>.
- [40] Wang YL, Holley AT, Ji C, Egolfopoulos FN, Tsotsis TT, Curran HJ. Propagation and extinction of premixed dimethyl-ether/air flames. *Proc Combust Inst* 2009;32:1035–42. <https://doi.org/10.1016/j.proci.2008.06.054>.
- [41] Egolfopoulos FN, Hansen N, Ju Y, Kohse-Höinghaus K, Law CK, Qi F. Advances and challenges in laminar flame experiments and implications for combustion chemistry. *Prog Energy Combust Sci* 2014; 43:36–67. <https://doi.org/10.1016/j.pecs.2014.04.004>.
- [42] D. Goodwin, H. Moffat, R. Speth, Cantera: An Object-oriented Software Toolkit for Chemical Kinetics, Thermodynamics, and Transport Processes, 2015. <http://dx.doi.org/10.5281/zenodo.48735>
- [43] K.J. Bosschaart and L.P.H. de Goey, The laminar burning velocity of flames propagating in mixtures of hydrocarbons and air measured with the heat flux method, *Comb. Flame* 136 (2004) 261–269. <https://doi.org/10.1016/j.combustflame.2003.10.005>.